

Topography of Spin Liquids on a Triangular Lattice

Zhenyue Zhu, P. A. Maksimov, Steven R. White, and A. L. Chernyshev

Department of Physics and Astronomy, University of California, Irvine, California 92697, USA



(Received 30 December 2017; revised manuscript received 12 February 2018; published 15 May 2018)

Spin systems with frustrated anisotropic interactions are of significant interest due to possible exotic ground states. We have explored their phase diagram on a nearest-neighbor triangular lattice using the density-matrix renormalization group and mapped out the topography of the region that can harbor a spin liquid. We find that this spin-liquid phase is continuously connected to a previously discovered spin-liquid phase of the isotropic $J_1 - J_2$ model. The two limits show nearly identical spin correlations, making the case that their respective spin liquids are isomorphic to each other.

DOI: [10.1103/PhysRevLett.120.207203](https://doi.org/10.1103/PhysRevLett.120.207203)

Introduction.—Some of the most visionary ideas prevail despite failing the original test case they were suggested to describe. Such is the seminal proposal of a spin liquid (SL) as a ground state of the nearest-neighbor (NN) $S = \frac{1}{2}$ triangular-lattice (TL) Heisenberg antiferromagnet [1]. Although the ground state of this model proved to be magnetically ordered [2,3], the concept of spin liquid remains highly influential in a much broader context [4,5].

The recent surge of activity [6–29] brings back the NN TL model as a potential holy grail of spin liquids that may provide a redemption to the original proposal of Ref. [1]. In its modern reincarnation, the key players are the highly anisotropic spin interactions, borne out of the strong spin-orbit coupling [6,8,25]. This ongoing effort is also inspired by the Kitaev SL construct for the honeycomb lattice [30], although without the benefit of an exact solution in the TL geometry.

The highly anisotropic interactions in the rare-earth compounds naturally emerge from a projection of the large magnetic moments onto the low-energy pseudospin- $\frac{1}{2}$ degrees of freedom [31]. Among the recently discovered TL rare-earth-based magnets, YbMgGaO₄ (YMGO) [6] received the most attention. While the debate on the intrinsic vs disorder-induced nature of its spin-liquid-like response is ongoing [7,16,26–28], a broader family of the TL rare-earth materials has become available [8,29].

Thus, it is important to provide a much needed framework to this area by establishing the phase diagram of the most general NN TL model with an unbiased numerical approach that goes beyond the mean-field methods that favor SL by design [7,11]. That should also settle whether extrinsic mechanisms are at work to mimic an SL behavior in the cases such as YMGO [16].

In this Letter, we explore the three-dimensional (3D) phase diagram of the most general NN model of these materials by using the density-matrix renormalization group (DMRG) aided by quasiclassical analysis. In

agreement with prior numerical work [16,17,25], we find that the phase diagram is dominated by well-ordered states and shows no indication that anisotropic terms by themselves can lead to a massive degeneracy that can favor SL states. On the contrary, most of the phase boundaries are nearly classical, implying reduced quantum fluctuations and strongly gapped states. Nonetheless, we have found a likely candidate for an SL state and created its topographic map. The maximal extent of the SL phase is achieved at the isotropic limit of the bond-independent part of the model, questioning that anisotropies are a prime source of an SL in these systems.

While the local character of the f -shell magnetism of the rare-earth ions dictates the dominance of the NN interactions, experiments suggest a sizable next-NN coupling J_2 [12,24]. We find that a four-dimensional extension of the phase diagram with J_2 allows for a natural continuity of the SL state from the anisotropic TL to the isotropic $J_1 - J_2$ limit [32–41]. The spin-spin correlations show no transition vs J_2 and are nearly identical between these two limits, suggesting isomorphism of the corresponding SL states. Our study indicates that these SLs are either Z_2 or Dirac-like [25,34–41], not the “spinon metal” SL state, argued to exist in YMGO [7,23].

Model.—The general NN TL model [6,8] with spin anisotropies constrained by the TL symmetries has both XXZ and bond-dependent terms, $\mathcal{H} = \mathcal{H}_{\text{XXZ}} + \mathcal{H}_{\text{bd}}$,

$$\begin{aligned} \mathcal{H}_{\text{XXZ}} &= J \sum_{\langle ij \rangle} (S_i^x S_j^x + S_i^y S_j^y + \Delta S_i^z S_j^z), \\ \mathcal{H}_{\text{bd}} &= \sum_{\langle ij \rangle} 2J_{\pm\pm} (\cos \tilde{\varphi}_\alpha[x, y]_{ij} - \sin \tilde{\varphi}_\alpha\{x, y\}_{ij}) \\ &\quad + J_{z\pm} (\cos \tilde{\varphi}_\alpha\{y, z\}_{ij} - \sin \tilde{\varphi}_\alpha\{x, z\}_{ij}), \end{aligned} \quad (1)$$

where $0 \leq \Delta \leq 1$ for layered systems, auxiliary phases are $\tilde{\varphi}_\alpha = \{0, -2\pi/3, 2\pi/3\}$ for bonds along the primitive

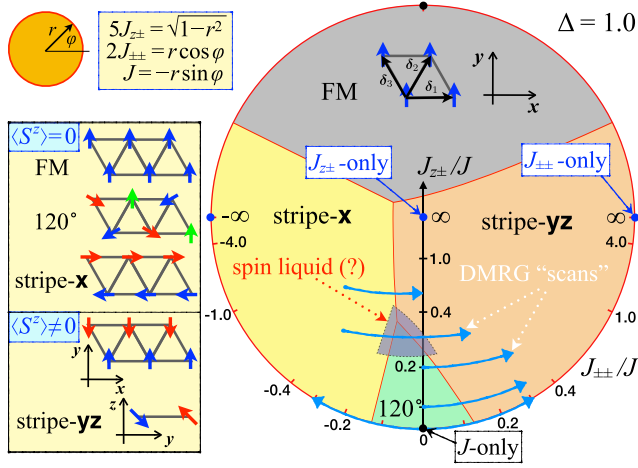


FIG. 1. The classical 2D phase diagram of the model (1) for $\Delta = 1.0$ using polar parametrization (see inset). The sketches of the ordered states (see text) and lattice primitive vectors are shown. Some of the DMRG scans of Figs. 2 and 3 are shown by arrows. The shaded triangle shows the SL phase. For the 3D phase diagram and phase boundaries, see SM [43].

vectors δ_α in Fig. 1, and notations $[a, b]_{ij} = S_i^a S_j^b - S_i^b S_j^a$ and $\{a, b\}_{ij} = S_i^a S_j^b + S_i^b S_j^a$ are used for brevity [42].

Classical phase diagram.—The XXZ term in (1) favors coplanar states: the well-known 120° state for $\Delta \leq 1$ and $J > 0$, and a ferromagnetic state for $J < 0$. The \mathcal{H}_{bd} terms in (1) are incompatible for different bonds [43], leave no continuous spin symmetries, and select “stripe-x” and “stripe-yz” as ground states [8,17]; see Fig. 1.

In the “stripe-x” state, favored by $J_{\pm\pm} < 0$, spins align along one bond in ferromagnetic “stripes” that order antiferromagnetically; see Fig. 1. This structure is only partially frustrated as the $J_{\pm\pm}$ term is fully satisfied on the x bond and half-satisfied on two other bonds [17,43]. The stripe-yz state benefits the $J_{\pm\pm} > 0$ and $J_{\pm\pm}$ terms in a similar manner. Here spins in ferromagnetic stripes are perpendicular to the fully satisfied x bond and are tilting out of the lattice plane with the angle dependent on the ratio $J_{\pm\pm}/J_{\pm\pm}$, reaching $\pi/4$ at $J_{\pm\pm} \rightarrow \infty$ [17]. The boundaries between all phases in Fig. 1 can be found analytically; see the Supplemental Material (SM), Ref. [43]. The results are identical for $J_{\pm\pm} < 0$ [8].

In Fig. 1, we present a two-dimensional (2D) cut of the classical 3D phase diagram of the NN TL model (1) at $\Delta = 1.0$ that shows all four phases discussed above. The full 3D phase diagram is a solid cylinder with the vertical axis $0 \leq \Delta \leq 1$ and the 2D cuts showing only quantitative changes vs Δ ; see the SM [43]. The polar parametrization maps the 2D parameter space onto a circle and the choice of numerical factors is to exaggerate the region $J_{\pm\pm}$, $J_{\pm\pm} \lesssim J$. In Fig. 1, we also identify an area of the suspected SL phase discussed below.

DMRG results.—To investigate the 3D phase diagram of the model (1) by DMRG we use several complementary

approaches. First is the long-cylinder 1D “scans,” in which one of the parameters is varied along the length of the cylinder and spin patterns provide a faithful visual extent of different phases that appear [16,34,45]. We use different boundary conditions and ranges of the varied parameter to exclude unwanted proximity effects [43]. Second are the shorter cylinders [46] with fixed parameters (“nonscans”) used as a probe for a sequence of points along the same 1D scans or at individual points of the phase diagram. Third is the $1/L$ scaling of the ordered moment using clusters with fixed aspect ratio [3]. We also use measurements of the correlation lengths and intensity maps of the structure factor, $\mathcal{S}(\mathbf{q})$ [43].

Figures 2 and 3 present our key results; see the SM [43] for details. In Fig. 2 we show 2D phase diagrams for $\Delta = 0.5$ and 1.0 , focusing on the region around the 120° phase. The circles with error bars are transitions observed in the scans, such as the ones shown in Figs. 3(a) and 3(b);

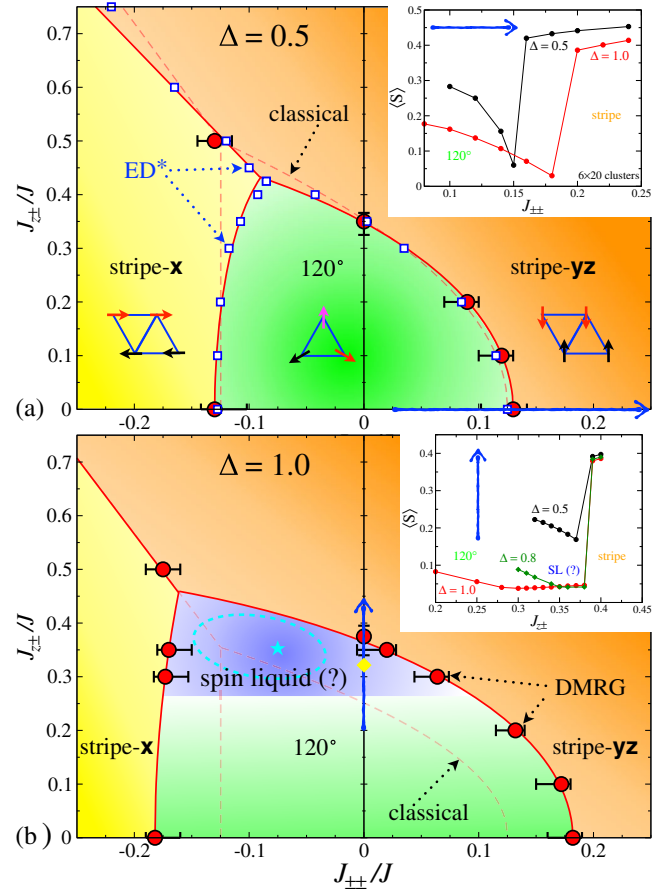


FIG. 2. The 2D phase diagrams for $\Delta = 0.5$ and 1.0 . The circles are from the 1D DMRG scans, see text and Fig. 3, squares are ED results [17], solid lines are guides to the eye, dashed lines are classical phase boundaries, arrows show parameter cuts for the insets. Insets show $\langle S \rangle$ vs $J_{\pm\pm}$ ($J_{\pm\pm}$) in units of J from cylinders with fixed parameters [46]. Stars are parameters used in $1/L$ scaling in Fig. 3(c); see text.

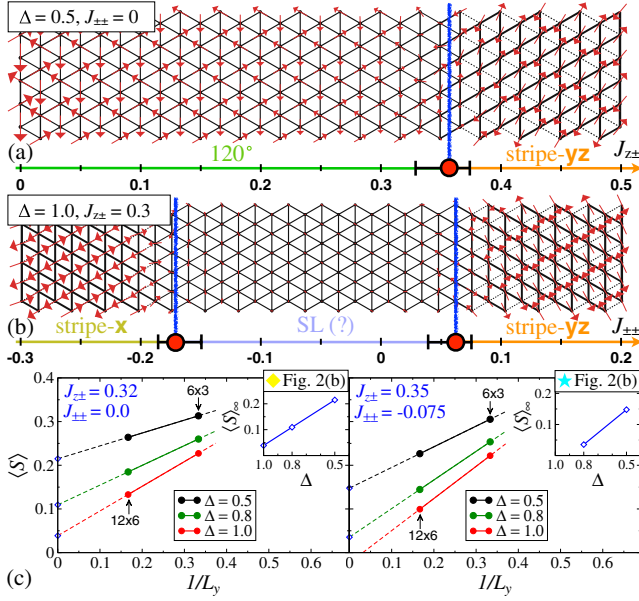


FIG. 3. The 1D DMRG scans [46] for (a) $\Delta = 0.5, J_{\pm\pm} = 0$ vs $J_{z\pm}$, and (b) $\Delta = 1.0, J_{z\pm} = 0.3$ vs $J_{\pm\pm}$ ($J_{\pm\pm}, J_{z\pm}$ in units of J). The circles and lines show transitions, arrows are the in-plane projections of $\langle S \rangle$. (c) The $1/L$ scaling of $\langle S \rangle$ for parameters marked with stars in Fig. 2(b). Insets show Δ dependencies of the extrapolated $\langle S \rangle_\infty$.

squares in Fig. 2(a) are the exact-diagonalization (ED) results from Ref. [17]; solid lines are guides to the eye.

Our scans for $\Delta = 0.5$ in Fig. 2(a) and the ED are remarkably close, both showing direct transitions between robust magnetic orders that are nearly coincident with the classical phase boundaries (dashed lines). The nonscan ordered moments, shown in the insets of Fig. 2 along two representative cuts, support these findings.

Figure 2(b) summarizes our results for the isotropic limit of the XXZ term (1), $\Delta = 1.0$. We find an expansion of the 120° phase beyond its classical boundaries with the transitions from it to the stripe phases remaining direct for $J_{z\pm} \lesssim 0.25$ [43]; see inset in Fig. 2(a). Here we find a possible SL state in the $J_{z\pm} \approx [0.27, 0.45]$ window; see also Fig. 3(b) and SM [43].

The inset of Fig. 2(b) presents the nonscan ordered moment $\langle S \rangle$ along the $J_{z\pm}$ cut. It shows a kink-like feature at $J_{z\pm} \approx 0.28$ for $\Delta = 1.0$. However, the intermediate phase from $J_{z\pm} \approx 0.28$ to 0.38 still exhibits a weak order. The same plot shows a similar feature for $\Delta = 0.8$ from $J_{z\pm} \approx 0.35$ to 0.38 while for $\Delta = 0.5$ the transition is direct. The scans for $\Delta = 0.8$ show the SL-suspect region that is significantly smaller than for $\Delta = 1.0$ [43]. We note that all transitions to stripe states that we observe are first-order like.

Another test of the SL region is provided by the $1/L$ scaling of the ordered moment $\langle S \rangle$ [3] in Fig. 3(c) for representative points indicated by the stars in Fig. 2(b). The insets of Fig. 3(c) show the Δ dependence of the

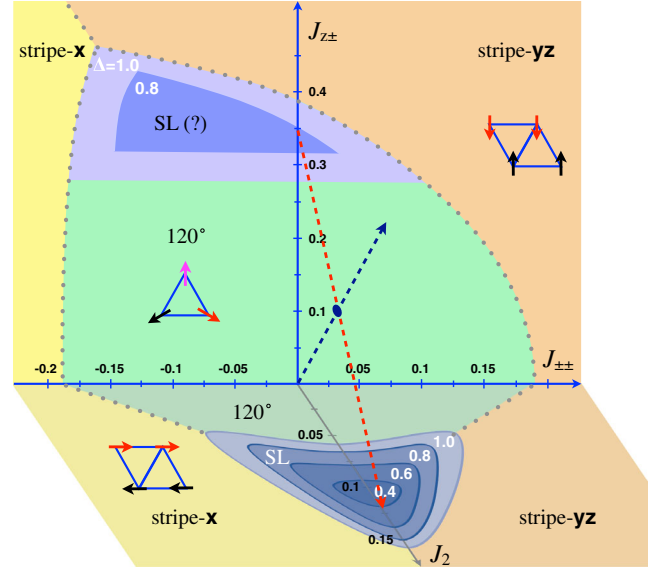


FIG. 4. Topographic maps of the SL regions of the 3D phase diagrams of the NN ($J_2 = 0$) model (1) (back panel) and of the J_1 - J_2 - $J_{\pm\pm}$ ($J_{z\pm} = 0$) XXZ model [16] (lower panel). Δ cuts are given in 0.2 increments and indicated. Dashed arrows show 1D DMRG cuts in Fig. 5.

extrapolated moment $\langle S \rangle_\infty$. This analysis suggests an SL state in a significantly smaller 3D region than the long-cylinder scans. Its approximate extent in the $\Delta = 1.0$ plane is shown in Fig. 2(b) by the dashed oval and it is limited along the XXZ axis by $\Delta \gtrsim 0.9$.

This should be compared with the J_1 - J_2 model, where different methods used here agree very closely on the extent of the SL region [16,34,43]. This is not the case in the present study, suggesting that a weak and/or more complicated form ordering [9] may persist in much of the suspected SL region.

We summarize the 3D quantum phase diagram for the model (1) in the back panel of Fig. 4 as a topographic map. It retains all classical phases of Fig. 1 and acquires an SL region. The generous outline of the latter represents a distorted conelike shape with the base at $\Delta = 1.0$ and the widest dimensions $J_{z\pm} \approx [0.27, 0.45]$ and $J_{\pm\pm} \approx [-0.17, 0.1]$ at that base. The tip of the cone extends along the XXZ axis down to $\Delta \gtrsim 0.7$. As is discussed above, the actual SL region may be significantly smaller. We also note that the SL phase occurs within the 120° region and its maximal extent is achieved at the isotropic limit of the XXZ term, questioning the importance of anisotropies for its existence.

J_2 extension.—Some of the most reliable experiments in YMGO strongly suggest that one should add a second-NN J_2 term to the NN model (1) [12,24]. The isotropic J_1 - J_2 model is also known to have an SL state for a range of $J_2 \approx [0.06, 0.16]J_1$ [33–41]. For both reasons, a minimal modification of the NN model (1) by the XXZ-only next-NN J_2 term suffices [43].

Recently, we have investigated the effect of the XXZ and $J_{\pm\pm}$ anisotropic terms on the J_1 - J_2 SL phase [16]. It survives down to $\Delta \approx 0.3$ and is eliminated completely by $|J_{\pm\pm}| \approx 0.1$. In the bottom panel of Fig. 4, we present a topographic map of the SL state in this XXZ J_1 - J_2 - $J_{\pm\pm}$ ($J_{z\pm} = 0$) model using results from Ref. [16].

Figure 4 suggests a connection between the SL phases of the anisotropic model (1) and of its isotropic J_1 - J_2 counterpart. We verify this connection for $\Delta = 1.0$ where the extent of both SL regions in Fig. 4 is maximal. We use two long-cylinder DMRG scans in the $J_{\pm\pm} = 0$ plane shown in Fig. 4 by arrows. The first scan connects the anisotropic SL at $J_{z\pm} = 0.35$ with the isotropic J_1 - J_2 SL at $J_2 = 0.12$ (units of J_1). The second scan starts at the origin (J_1 -only model) and is used to confirm the existence of an SL state between the 120° and the stripe phases along the direction tilted from the J_2 and $J_{z\pm}$ axes. For a different picture of these cuts, see the SM [43].

Figures 5(a) and 5(b) show the real-space images of these scans; dashed arrows are marking their crossing point; both coordinates ($J_{z\pm}, J_2$) are indicated. The first cylinder has an open boundary condition and one site removed at each end to suppress spinon localization at the edge [34,43]. The scan shows no indication of magnetic, chiral, or valence-bond order [43] and no change of the SL state along the cylinder, the latter inferred from the thickness of the bonds that are proportional to the nearest-neighbor correlation $\langle \mathbf{S}_i \mathbf{S}_j \rangle$. The second scan, Fig. 5(b), shows a transition from the 120° to the stripe- yz state via an SL state, consistent with the first scan and also with the results in Figs. 2(b) and 4 and Refs. [16,43] for the scans along $J_{z\pm}$ and J_2 axes.

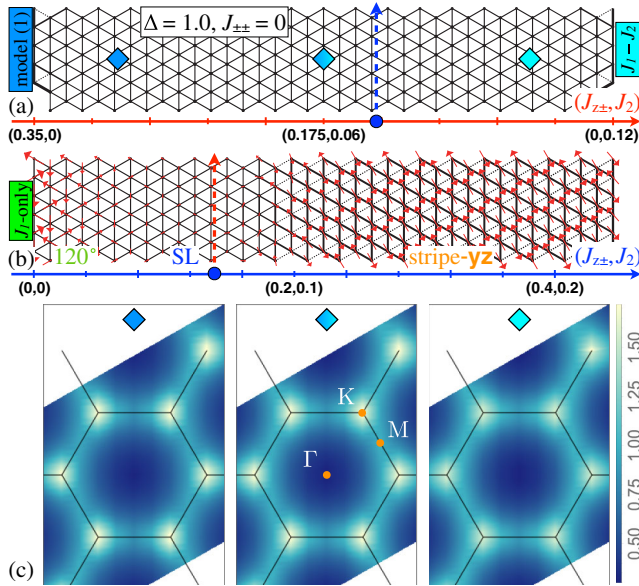


FIG. 5. (a),(b) DMRG scans at $\Delta = 1.0$ as shown in Fig. 4. $J_{z\pm}, J_2$ are in units of J_1 ; the crossing point of the scans in Fig. 4 is shown by blue dots and dashed arrows. (c) $S(\mathbf{q})$ maps from three sections of the cylinder in (a) marked by the diamonds.

To infer the character of the SL states, we calculate the static structure factor, $S(\mathbf{q})$, using correlations from the three sections of the cylinder in Fig. 5(a) with centers of these sections marked by the diamonds [47]. The first section represents the region that is close to the limit of the original anisotropic model (1), the third section is close to the isotropic J_1 - J_2 SL, and the second is in between. The results are shown in Fig. 5(c) where $S(\mathbf{q})$ is at $q_z = 0$ [48]. We have also calculated $S(\mathbf{q})$ in nonscan cylinders for the limits of the scan in Fig. 5(a) as well as at other points within the SL regions in Fig. 4 with quantitatively very similar results [43].

The structure factors in Fig. 5(c) are nearly identical, implying that the SLs in the anisotropic model (1) and in the isotropic J_1 - J_2 model, as well as any SL state in between, are isomorphic to each other [49]. The correlations show a broadened peak at the K points, the feature consistent with the Z_2 [34–36], U(1) Dirac [37], or Dirac-like [25,38–41] SLs, but not with the spinon Fermi surface SL state proposed for YMGO [7,23]. This suggests that an extrinsic mechanism is responsible for an SL-like response in this material. The YMGO structure factor has maxima of intensity at the M points, the feature readily obtainable from stripe domains of mixed orientations, see [43], supporting the SL mimicry scenario of Ref. [16].

Summary.—We have explored the 3D phase diagram of the anisotropic NN model (1) on an ideal TL lattice using DMRG. We have identified an SL region of the phase diagram and created its topographic map. This SL state occurs at the border between 120° and stripe phases, with its maximal extent reached at the isotropic limit of the XXZ term. We have studied a four-dimensional extension of the phase diagram by the next-NN J_2 term and have shown that it connects the newly found SL state to the well-known isotropic J_1 - J_2 model. The spin-spin correlations are nearly identical everywhere between these two limits, suggesting a complete isomorphism of the corresponding SL states. This also rules out the “spinon metal” SL state as a viable candidate for materials that realize an anisotropic TL model.

We thank Professor Xiaoqun Wang and Dr. Qiang Luo for sending their published data from Ref. [17], Itamar Kimchi for sharing his notes prior to publication and a discussion, and Cecile Repellin for sharing unpublished results and a useful conversation. We are grateful to George Jackeli for a patient discussion and support and to Natalia Perkins for a useful technical tip. We are indebted to Martin Mourigal for numerous communications, explanations, indispensable comments, and unique insights. This work was supported by the U.S. Department of Energy, Office of Science, Basic Energy Sciences under Award No. DE-FG02-04ER46174 (P. A. M. and A. L. C.) and by the NSF through grant DMR-1505406 (Z. Z. and S. R. W.).

- [1] P. W. Anderson, *Mater. Res. Bull.* **8**, 153 (1973); P. Fazekas and P. W. Anderson, *Philos. Mag.* **30**, 423 (1974).
- [2] L. Capriotti, A. E. Trumper, and S. Sorella, *Phys. Rev. Lett.* **82**, 3899 (1999).
- [3] S. R. White and A. L. Chernyshev, *Phys. Rev. Lett.* **99**, 127004 (2007).
- [4] L. Savary and L. Balents, *Rep. Prog. Phys.* **80**, 016502 (2017).
- [5] L. Balents, *Nature (London)* **464**, 199 (2010).
- [6] Y. Li, H. Liao, Z. Zhang, S. Li, F. Jin, L. Ling, L. Zhang, Y. Zou, L. Pi, Z. Yang, J. Wang, Z. Wu, and Q. Zhang, *Sci. Rep.* **5**, 16419 (2015).
- [7] Y. Li, G. Chen, W. Tong, Li Pi, J. Liu, Z. Yang, X. Wang, and Q. Zhang, *Phys. Rev. Lett.* **115**, 167203 (2015).
- [8] Y.-D. Li, X. Wang, and G. Chen, *Phys. Rev. B* **94**, 035107 (2016).
- [9] C. Liu, R. Yu, and X. Wang, *Phys. Rev. B* **94**, 174424 (2016).
- [10] Y. S. Li, D. Adroja, P. K. Biswas, P. J. Baker, Q. Zhang, J. J. Liu, A. A. Tsirlin, P. Gegenwart, and Q. M. Zhang, *Phys. Rev. Lett.* **117**, 097201 (2016).
- [11] Y. Shen, Y.-D. Li, H. Wo, Y. Li, S. Shen, B. Pan, Q. Wang, H. C. Walker, P. Steffens, M. Boehm, Y. Hao, D. L. Quintero-Castro, L. W. Harriger, M. D. Frontzek, L. Hao, S. Meng, Q. Zhang, G. Chen, and J. Zhao, *Nature (London)* **540**, 559 (2016).
- [12] J. A. M. Paddison, M. Daum, Z. Dun, G. Ehlers, Y. Liu, M. B. Stone, H. Zhou, and M. Mourigal, *Nat. Phys.* **13**, 117 (2017).
- [13] Y.-D. Li, Y. Shen, Y. Li, J. Zhao, and G. Chen, *Phys. Rev. B* **97**, 125105 (2018).
- [14] Y. Xu, J. Zhang, Y. S. Li, Y. J. Yu, X. C. Hong, Q. M. Zhang, and S. Y. Li, *Phys. Rev. Lett.* **117**, 267202 (2016).
- [15] Y. D. Li, Y.-M. Lu, and G. Chen, *Phys. Rev. B* **96**, 054445 (2017).
- [16] Z. Zhu, P. A. Maksimov, S. R. White, and A. L. Chernyshev, *Phys. Rev. Lett.* **119**, 157201 (2017).
- [17] Q. Luo, S. Hu, B. Xi, J. Zhao, and X. Wang, *Phys. Rev. B* **95**, 165110 (2017).
- [18] Y. Li, D. Adroja, R. I. Bewley, D. Voneshen, A. A. Tsirlin, P. Gegenwart, and Q. Zhang, *Phys. Rev. Lett.* **118**, 107202 (2017).
- [19] Y. D. Li and G. Chen, *Phys. Rev. B* **96**, 075105 (2017).
- [20] Y. Li, D. Adroja, D. Voneshen, R. I. Bewley, Q. Zhang, A. A. Tsirlin, and P. Gegenwart, *Nat. Commun.* **8**, 15814 (2017).
- [21] S. Tóth, K. Rolfs, A. R. Wildes, and C. Rüegg, *arXiv:1705.05699*.
- [22] Z.-X. Luo, E. Lake, J.-W. Mei, and O. A. Starykh, *Phys. Rev. Lett.* **120**, 037204 (2018).
- [23] Y. Shen, Y.-D. Li, H. C. Walker, P. Steffens, M. Boehm, X. Zhang, S. Shen, H. Wo, G. Chen, and J. Zhao, *arXiv:1708.06655*.
- [24] X. Zhang, F. Mahmood, M. Daum, Z. Dun, J. A. M. Paddison, N. J. Laurita, T. Hong, H. Zhou, N. P. Armitage, and M. Mourigal, *arXiv:1708.07503*.
- [25] J. Iaconis, C. Liu, G. B. Halász, and L. Balents, *SciPost Phys.* **4**, 003 (2018).
- [26] Z. Ma *et al.*, *Phys. Rev. Lett.* **120**, 087201 (2018).
- [27] I. Kimchi, A. Nahum, and T. Senthil, *arXiv:1710.06860*.
- [28] E. Parker and L. Balents, *arXiv:1801.06941*.
- [29] M. B. Sanders, F. A. Cevallos, and R. J. Cava, *Mater. Res. Express* **4**, 036102 (2017).
- [30] A. Kitaev, *Ann. Phys. (Amsterdam)* **321**, 2 (2006).
- [31] J. S. Gardner, M. J. P. Gingras, and J. E. Greedan, *Rev. Mod. Phys.* **82**, 53 (2010).
- [32] C. J. Gazza and H. A. Ceccatto, *J. Phys. Condens. Matter* **5**, L135 (1993).
- [33] P. H. Y. Li, R. F. Bishop, and C. E. Campbell, *Phys. Rev. B* **91**, 014426 (2015).
- [34] Z. Zhu and S. R. White, *Phys. Rev. B* **92**, 041105 (2015).
- [35] W.-J. Hu, S.-S. Gong, W. Zhu, and D. N. Sheng, *Phys. Rev. B* **92**, 140403 (2015).
- [36] D.-V. Bauer and J. O. Fjærestad, *Phys. Rev. B* **96**, 165141 (2017).
- [37] Y. Iqbal, W.-J. Hu, R. Thomale, D. Poilblanc, and F. Becca, *Phys. Rev. B* **93**, 144411 (2016).
- [38] R. Kaneko, S. Morita, and M. Imada, *J. Phys. Soc. Jpn.* **83**, 093707 (2014).
- [39] S.-S. Gong, W. Zhu, J.-X. Zhu, D. N. Sheng, and K. Yang, *Phys. Rev. B* **96**, 075116 (2017).
- [40] S. N. Saadatmand and I. P. McCulloch, *Phys. Rev. B* **94**, 121111 (2016).
- [41] R. V. Mishmash, J. R. Garrison, S. Bieri, and C. Xu, *Phys. Rev. Lett.* **111**, 157203 (2013).
- [42] For a less humane form of (1), see, e.g., [7]. We use a standard form of the XXZ term (cf. [7] and others) with $J = 2J_{\pm}$ and anisotropy $\Delta = J_z/2J_{\pm}$ in their notations and a different operator form in \mathcal{H}_{bd} (1).
- [43] See Supplemental Material at <http://link.aps.org/supplemental/10.1103/PhysRevLett.120.207203>, which includes Refs. [44], for technical details on the model, additional DMRG and spin-wave theory results.
- [44] A. Biffin, R. D. Johnson, I. Kimchi, R. Morris, A. Bombardi, J. G. Analytis, A. Vishwanath, and R. Coldea, *Phys. Rev. Lett.* **113**, 197201 (2014).
- [45] Z. Zhu, D. A. Huse, and S. R. White, *Phys. Rev. Lett.* **110**, 127205 (2013); **111**, 257201 (2013).
- [46] Long cylinders are 6×30 or 6×36 sites and shorter cylinders with fixed parameters are 6×12 and 6×20 sites. We keep up to $M = 1600$ or 2000 states depending on the complexity of the Hamiltonian.
- [47] $\mathcal{S}(\mathbf{q}) = \sum_{\alpha\beta} (\delta_{\alpha\beta} - q_{\alpha}q_{\beta}/q^2) S_{\mathbf{q}}^{\alpha\beta}$ is obtained from the spin-spin correlation function $S_{\mathbf{q}}^{\alpha\beta} = \sum_{i,j} \langle S_i^{\alpha} S_j^{\beta} \rangle e^{i\mathbf{q}(\mathbf{R}_i - \mathbf{R}_j)}$.
- [48] No significant variation is detected vs q_z .
- [49] $\mathcal{S}(\mathbf{q})$ intensity maps in Fig. 5(c) are nearly identical, with the largest discrepancy $< 5\%$ in the entire Brillouin zone. Individual real-space $\langle S_i^{\alpha} S_j^{\beta} \rangle$ correlations with distances $|r_{ij}|$ up to $6a$ are also nearly identical [43].